PLOS ONE |

RESEARCH ARTICLE

Elastic modulus and toughness of orb spider glycoprotein glue

Brent D. Opell*, Mary E. Clouse, Sheree F. Andrews

Department of Biological Sciences, Virginia Tech, Blacksburg, Virginia, United States of America

* bopell@vt.edu

Abstract

An orb web's prey capture thread features tiny glue droplets, each formed of an adhesive glycoprotein core surrounded by an aqueous layer. Small molecules in the aqueous layer confer droplet hygroscopicity and maintain glycoprotein viscoelasticity, causing droplet volume and glycoprotein performance to track changes in environmental humidity. Droplet extension combines with that of a thread's supporting flagelliform fibers to sum the adhesive forces of multiple droplets, creating an effective adhesive system. We combined measurements of the force on an extending droplet, as gauged by the deflection of its support line, with measurements of glycoprotein volume and droplet extension to determine the Young's modulus (*E*) and toughness of three species' glycoproteins. We did this at five relative humidities between 20–90% to assess the effect of humidity on these properties. When droplets of a thread span extend, their extensions are constrained and their glycoprotein filaments remain covered by aqueous material. This was also the case during the first extension phase of the individual droplets that we examined. However, as extension progressed, the aqueous layer was progresses disrupted, exposing the glycoprotein. During the first extension phase *E* ranged from 0.00003 GPa, a value similar to that of fibronectin, a glycoprotein that anchors cells in the extracellular matrix, to 0.00292 GPa, a value similar to that of resilin in insect ligaments. Second phase *E* increased 4.7–19.4-fold. When compared at the same humidity the *E* of each species' glycoprotein was less than 5% of the value reported for its flagelliform fibers. This difference may facilitate the coordinated extension of these two capture thread components that is responsible for summing the thread's adhesive forces.

OPEN ACCESS

Citation: Opell BD, Clouse ME, Andrews SF (2018) Elastic modulus and toughness of orb spider glycoprotein glue. PLoS ONE 13(5): e0196972. https://doi.org/10.1371/journal.pone.0196972

Editor: Jui-Yang Lai, Chang Gung University, TAIWAN

Received: December 11, 2017

Accepted: April 24, 2018

Published: May 30, 2018

Copyright: © 2018 Opell et al. This is an open access article distributed under the terms of the Creative Commons Attribution License, which permits unrestricted use, distribution, and reproduction in any medium, provided the original author and source are credited.

Data Availability Statement: A summary of the data are provided in eight supplementary tables and an Excel file containing the full data set is also provided.

Funding: National Science Foundation grant IOS-1257719 (BO) supported this study. The funders had no role in study design, data collection and analysis, decision to publish, or preparation of the manuscript.

Competing interests: The authors have declared that no competing interests exist.

Introduction

The multiple uses that spiders make of their proteinaceous silk threads have made an important contribution to the success of this 47,055-species clade [1–6]. Nowhere is this more evident than in the intricate webs constructed by orb weaving spiders of the superfamily Araneoidea (Fig 1A). Along with their descendants that construct webs of divergent architectures, members of this clade comprise 26% of all living spider species [7–9]. These orb webs are the products of four different silk glands, each opening at the tip of a spigot on one of the

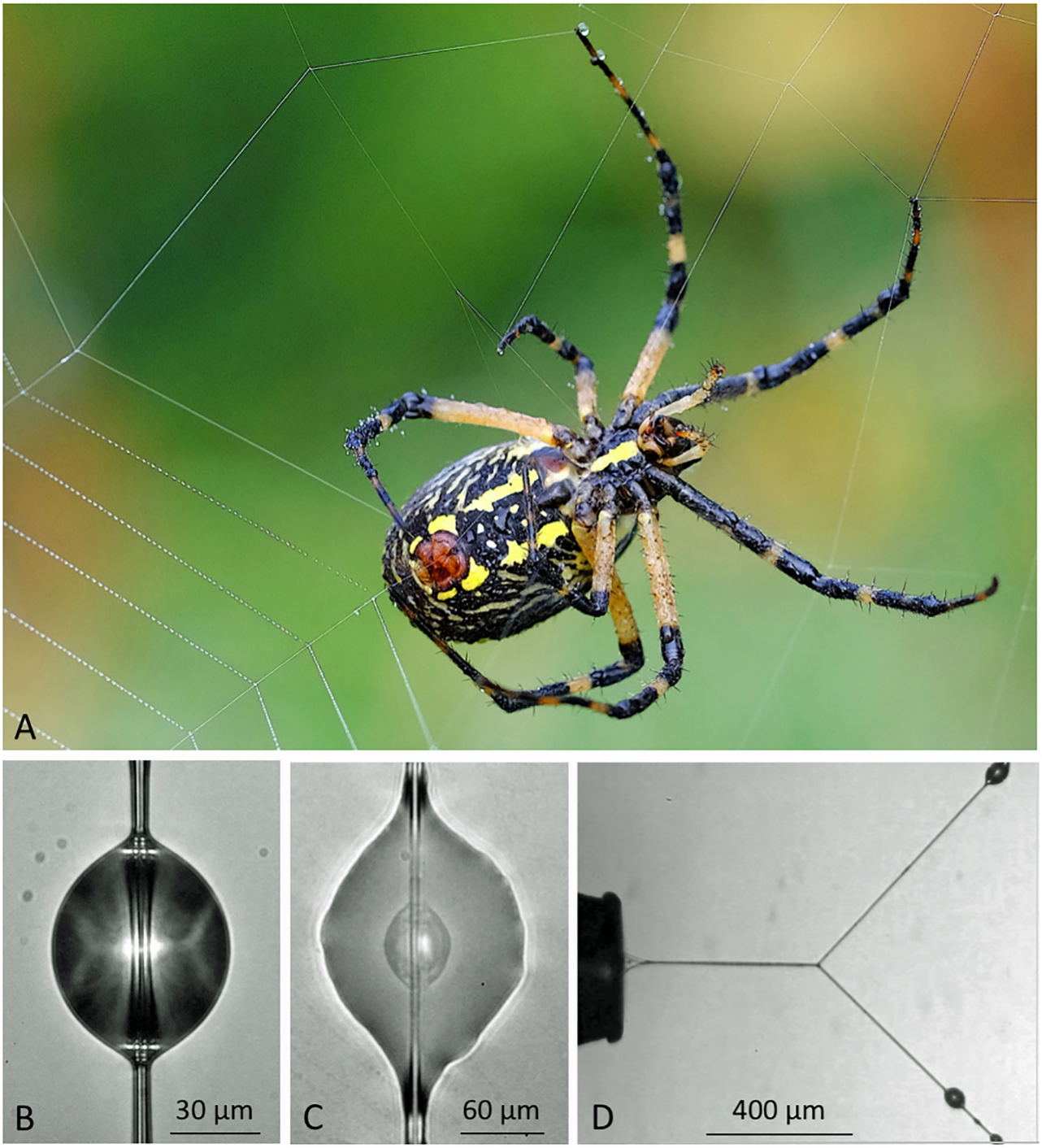

Fig 1. Viscous prey capture threads and their droplets. A. *Argiope aurantia* female depositing a capture thread. B. A suspended *A. aurantia* viscous droplet, showing paired flagelliform axial fibers, as magnified by the droplet's curved surface, C. A flattened *N. crucifera* droplet showing a glycoprotein core attached to axial fibers and surrounded by aqueous material. D. An extended *N. crucifera* droplet, which has deflected its support line.

https://doi.org/10.1371/journal.pone.0196972.g001

spider's six spinnerets [10]. Attached by pyriform gland disks [11], threads from the major ampullate glands form the web's strong, but stiff frame and radial lines that absorb and dissipate the kinetic energy of prey strikes [12–14]. Adhesive viscous prey capture threads are laid as a spiral on the web's radii and prevent insects from escaping the web before a spider can

locate, run to, and subdue them [15, 16]. These composite threads are produced by two types of silk glands that open on adjacent spigots on a spider's paired posterior lateral spinnerets [17]. On each spinneret, two aggregate gland spigots flank a flagelliform gland spigot. As a flagelliform fiber emerges, it is coated with aqueous aggregate gland material. Threads from the two spinnerets merge and Plateau Rayleigh instability quickly reconfigures the cylinder of aggregate material that surrounds the two flagelliform fibers into a series of regularly spaced droplets, a core of adhesive glycoprotein coalescing inside of each droplet Fig 1A–1C) [18–20].

Unlike the anchoring adhesives of mussels and barnacles, which are enzymatically toughened to resist crack propagation that leads to failure [21–24], orb spider glycoprotein glue has evolved as a compliant, extensible adhesive (Fig 1D), a feature that is critical for a thread's adhesion. As a struggling insect pulls on an attached capture thread, individual droplets extend, transferring force to the axial line, causing it to bow and assume a parabolic configuration (Fig 2). Thus, in suspension bridge fashion, the adhesion generated by multiple droplets is summed over a thread span [25, 26]. Hygroscopic low molecular mass compounds (LMMCs) and inorganic salts in the aqueous layer that surrounds a thread's axial fibers and glycoprotein core facilitate thread adhesion in two ways. These compounds attract atmospheric moisture [27–30], which ensures the extensibility of both glycoprotein and axial fibers [31–34]. LMMCs also maintain the glycoprotein's structure and enhance its surface interactions [35]. Under light microscopy proteins are visible only in the droplet's core (Fig 1C). However, along with LMMCs, proteins are also present in the droplet's aqueous layer [35].

Major ampullate threads, flagelliform axial fibers, and glycoprotein are all spidroins, members of the spider fibroin gene family of scleropoteins [4, 36–41]. Since orb weavers first spun viscous threads in the early cretaceous [42] the material properties and these threads and of major ampullate threads appear to have evolved in consort, tuning each to their role in prey capture. Consistent with their role of absorbing the force of prey impact, major ampullate threads are stiffer than flagelliform fibers, which support viscous capture threads [12]. Stiffness, more formally termed elastic modulus or Young's modulus (E), describes a material's resistance to being deformed elastically. Major ampullate threads have E values of 3.4–11.5 GPa and flagelliform fibers values of 0.012–0.08 GPa [12]. We hypothesize that to effectively implement a suspension bridge mechanism of adhesive recruitment glycoprotein E should be less than that of flagelliform fibers, whose values differ among species [12]. If glycoprotein is too stiff relative to a thread's flagelliform fibers then the outer droplets of a contacting strand will release before inner droplets have extended and contributed their adhesion. To test this hypothesis we constructed stress-strain curves for three species' viscous droplets and used these curves to determine E of the droplet's glycoprotein cores. These curves also permitted us to determine the glycoprotein core's toughness, the work required to extend the material to rupture, or, in the case of viscous threads droplets, pull-off from a contacted surface. This is an important index because droplet and axial line extension dissipate the energy of an insect's struggles to escape from a web [43].

Under the high humidity of early morning and evening, when most orb webs are constructed, hygroscopic compounds in a viscous thread aggregate material attracts atmospheric moisture, which contributes to the volume and instability of the aggregate cylinder that initially covers the axial fibers. After droplets and their glycoprotein cores form, these compounds remain in the aqueous layer, causing droplet volume and glycoprotein volume and viscosity to track changes in environmental humidity [17, 32, 44]. For species that occupy humid streamside or forest habitats little hygroscopicity is necessary to achieve a balance between glycoprotein adhesion and cohesion that optimizes thread adhesion [44]. In fact, hygroscopicity that is excessive reduces viscosity and leads to cohesive failure [32, 34]. However, for species that live in exposed habitats where humidity drops during the day, greater thread hygroscopicity is

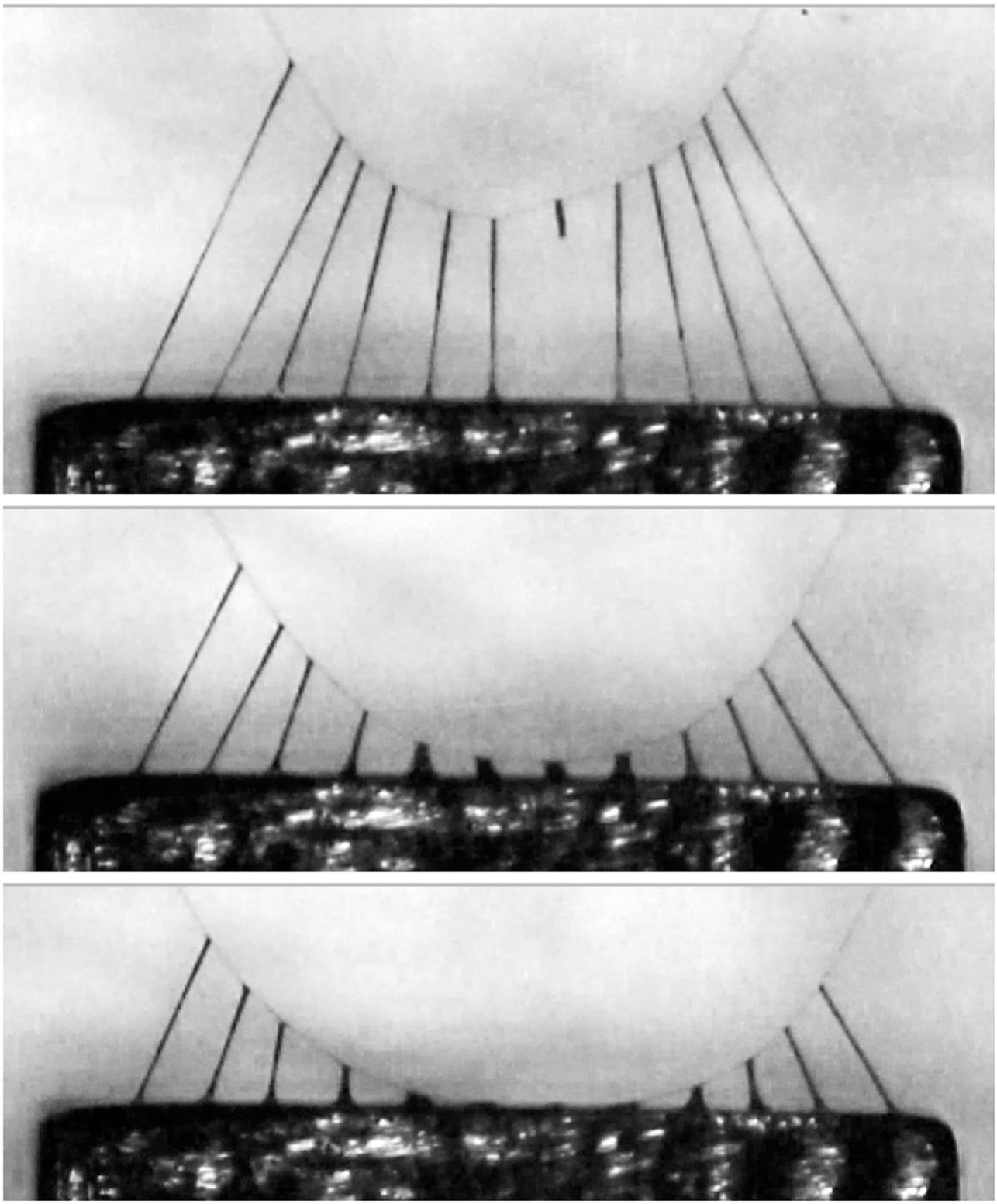

Fig 2. Video screen captures of a *V. arenata* capture thread being progressively pulled (bottom to top) from a 2mm wide contact plate. Force from the thread's extending droplets is summed by its deflected axial line. In the top frame a droplet near the strand's center has released from the plate, introducing an instability that will initiate adhesive failure. Thread release is more typically initiated when peripheral droplets release. Middle and top figures from Opell et al., 2018.

https://doi.org/10.1371/journal.pone.0196972.g002

necessary to maintain glycoprotein viscosity. When the adhesion of five species' capture threads were measured at different humidities, each registered the greatest value at its typical foraging humidity, but at these optimal humidities all species had similar glycoprotein viscosities [44]. Thus, natural selection has tuned the viscosity of an orb spider's glycoprotein glue to the humidity of its habitat by adjusting the composition and concentration of LMMCs and salts that determine the aqueous layer' hygroscopicity. To complete this picture, we characterized the *E* and toughness of glycoproteins from three of the five species included in this previous study at five humidities ranging from 20–90% relative humidity (RH). Although viscosity and elastic modulus are both affected by glycoprotein cohesion, they are not interchangeable indices. Viscosity was measured from the spreading velocity of glycoprotein on a glass surface while it remained within its native aqueous layer [44], whereas we determined Young's modulus by extending droplets to pull-off. As physical and covalent bonds appear responsible for glycoprotein cohesion [33, 34] glycoprotein flow is unlikely to disrupt these bonds; whereas extension affords an opportunity for glycoprotein molecules to unfold and for sacrificial bonds to break [45].

The *E* and toughness of a material is determined from its stress-strain curve, which requires simultaneously measuring the force on the material and its elongation as it is extended to the point of failure. However, the small size of a viscous droplet's glycoprotein core (Fig 1C; 821–8,625 μm^3 at 55% relative humidity for the three species that were studied) makes it difficult to directly measure the force on single extending glycoprotein (Fig 1D). Moreover, the distribution of forces across the extending droplets of a capture thread strand is complicated [26], making it difficult to determine the force on a single droplet from the force on the entire strand. We met this challenge by using the deflection of a thread's axial line to gauge the force on a droplet during its video-captured extension (Fig 1D).

Methods and materials

Species studied and spider welfare

We studied three orb weaving species: *Verrucosa arenata* (Walckenare, 1841), a diurnal species that occupies humid forests, *Neoscona crucifera* (Lucas, 1838), a nocturnal species that is found in vegetation on forest edges, where it constructs webs shortly after dusk, but continues to forage during the following day, and *Argiope aurantia* Lucas, 1833, a dirunal species found in weedy vegetation where its web experiences low humidity during the late morning and afternoon [32]. These are common and abundant species that are neither threatened nor endangered. Threads from webs constructed by 12, 14, and 14 adult females, respectively, of these species were collected from property near Blacksburg, Montgomery County, Virginia that is owned by Virginia Tech. Permission for this activity was granted by Virginia Tech's Department of Biological Sciences, College of Science, and Office of Sponsored Programs during the review and approval of the protocols described in the research grant that supported this study. This review and the project's approval by the United States National Science Foundation (NSF) ensured that the procedures we used complied with both Virginia Tech and NSF policies for the ethical use of animals in research studies. Only one web sample was collected from each individual spider. Spiders were not collected. Each spider either ran to or was chased unharmed to the edge of her web before a web sample was taken. The spider was, therefore, able to use the remainder of her web during the day of our collection and to construct a new web on the following day. Consequently, the impact of our thread sampling protocol on an individual spider was no greater than that of a single rainy day, which damaged her web or prevented her from spinning a new web.

Thread collection and preparation

We collected sectors from orb-webs soon after they were constructed to ensure threads were not contaminated by dust or pollen. *Neoscona crucifera* samples were collected between 21:00 and 22:00 and *A*. *aurantia* and *V*. *arenata* between 06:00 and 08:30. We marked the position of each sampled web with flagging tape to prevent resampling. Web sectors were collected using either an 18-cm diameter aluminum ring or on a 15 x 52 cm rectangular aluminum frame. Double-sided 3M tape (3M #9086K29550360) applied to the 0.6 cm width of the ring and center bar and on the 1.2 cm wide rectangular frame secured the threads without altering the original structure and tension of the web's threads. Immediately after collecting a web sample the ring or frame was placed in a closed container to prevent contamination. All images and videos described in the following sections were completed by 16:00 on the day web samples were collected. Procedures for characterizing droplets have been described [26, 31, 32, 46, 47] and are summarize here.

We prepared two sets of thread samples from each web, one used to determine the volume of the glycoprotein core within a droplet and one used to measure droplet extension. Threads on both samplers spanned a 4.8 mm space between supports that were covered with double-sided carbon tape (Cat #77816, Electron Microscope Sciences, Hatfield PA) to secure threads at their native tensions. On samplers used for droplet extension, we used a minuten insect pin moistened with water to slide droplets away from a focal droplet located at the strand's center.

Establishing test conditions

We photographed and extended droplets inside a glass covered chamber where temperature was maintained at 23˚ C. We monitored humidity with a Fisher Scientific® Instant Digital Hygrometer and established 20% and 37% RH's by placing a small Petri dishes with silica gel beads inside the chamber and 55%, 72% and 90% RH's by substituting a distilled water saturated Kimwipe®. We made small increases in RH by forcing air through a glass cylinder packed with distilled water saturated Upsorb sheets (Diversified Biotech) into the chamber and small increases in RH by drawing room air (~ 50% RH) into the chamber.

Determining droplet and glycoprotein volume

At each humidity, we photographed three suspended droplets and then flattened them by dropping a glass coverslip onto them from a release mechanism contained within the observation chamber, revealing each droplet's glycoprotein core (Fig 1C). Using ImageJ [48] we measured the lengths (DL; dimension parallel to the axial fiber) and widths (DW) of three suspended droplets and the surface area of each flattened droplet and its glycoprotein core. We computed suspended droplet volume (DV using the following formula [49, 50].

$$DV = (2\pi * DW^2 * DL)/15 \quad (1)$$

We divided by a droplet's surface area by its flattened surface area (GA) to determine its thickness, which was multiplied by glycoprotein surface area to determine glycoprotein volume (GV). For each individual and each test humidity, the mean glycoprotein-volume-to-droplet-volume ratio of three droplets was multiplied by volume this individual's extended droplet(s) (one droplet for *A*. *aurantia* and *N*. *crucifera* and two droplets for *V*. *arenata*) to infer the volume of this droplet's glycoprotein core.

Neoscona crucifera droplets did not flatten or adhere at 20% RH and, therefore, no values are available for this humidity. At 20% RH the glycoprotein cores of *V*. *arenata* did not flatten but appeared as spheres. Although cores flatten progressively as humidity increased, they

continued to remained elevated above the droplets flattened aqueous layer. Therefore, we computed V. arenata glycoprotein volume as described below.

1. We determined the radius (R) of the glycoprotein core from its measured surface area (GA) as if this were an image of a bisected sphere using the formula:

$$R = \sqrt{GA}/\pi \tag{2}$$

2. We determined the glycoprotein core's spherical volume (GSV) of the glycoprotein core using the formula:

$$GSV = \frac{4}{3}\pi\ R^3 \tag{3}$$

3. We next used the following formula to compute an adjusted glycoprotein volume (AGV) that accounted for progressive glycoprotein volume as humidity increased.

$$AGV = GSV * (GA/GA\ at\ 20\%\ RH) \tag{4}$$

S1 Fig compares *V*. *arenata* AGV and GV to those of the other two species' GV's, confirming that AGV proved a more appropriate index for this species, which increased rather than decreased with rising humidity. S2 Fig confirms that in all three species the thickness of flattened droplets decreases as humidity increases.

Extending droplets

The droplet observation chamber rested on the stage of a Mitutoyo FS60 inspection microscope (Mitutoyo America Corp., Aurora, IL, USA) (Fig 3). We photographed each droplet prior to extension. After cleaned the 413 μm wide polished steel tip of the probe with 100% ethanol on a Kimwipe®, the probe was inserted through a port in the side of the chamber, aligned with a thread droplet and anchored so that it remained stable. The microscope's stage was then advanced 500 μm, pressing the droplet against the probe tip and ensuring adhesion. A stepping motor attached to the microscope's mechanical stage then withdrew the thread at a velocity of 69.6 μm s^{-1} while a 60-fps video recorded the droplet's extension.

Computing glycoprotein Young's modulus and toughness

The seven steps involved in determining the stress and strain of each viscous thread droplet at each of the four points during its extension are described in Fig 3. These include determining the: 1. Length of the elongated axial line on each side of the extended droplet as the hypotenuse of a right triangle, with the side opposite θ/2 being the initial, upstretched 2400 μm length, 2. Amount of axial line extension relative to the initial 2400 μm length each half of the axial line, 3. Force on the axial line as the result of this extension, determined from values for each of the paired axial line fibers provided in the table included in Fig 4, 4. Force on the extended droplet filament determined by resolving the force vectors of the two axial line halves, 5. Cross sectional area of the extended glycoprotein filament, determined by dividing the inferred volume of a droplet's glycoprotein core by the extended droplet length, 6. True stress on the extended filament, determined by dividing the force on the extended glycoprotein filament by the filament's cross sectional area and 7. True strain on the extended glycoprotein filament, expressed

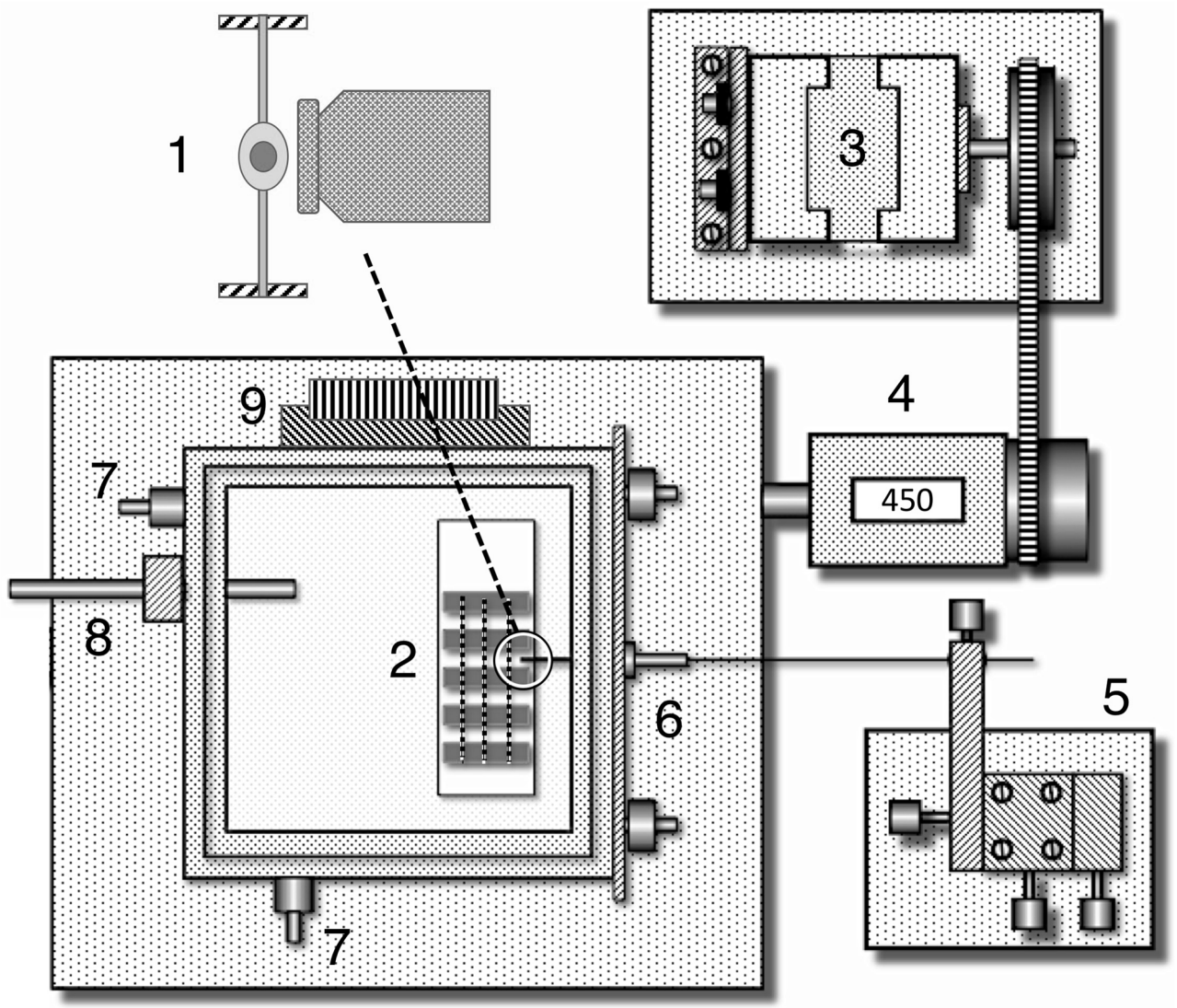

Fig 3. Components of the droplet extension system. 1. An isolated droplet suspended between supports with the probe's tip positioned and ready to contact droplet. 2. Microscope slide sampler within the glass-covered humidity and temperature controlled temperature chamber resting on the microscope's mechanical stage. 3. Stepping motor used to activate the mechanical stage's X manipulator, which pushes the stage to the left of the image. 5. Stationary device that holds the probe stationary as the stage is moved. 6. Adjustable plate with a port for the probe to pass through, enabling the probe tip to be aligned with a thread droplet before the probe is stabilized. 7. Intake and outlet ports used to draw dehumidified air or room air into the observation chamber. 8. Hygrometer probe used to monitor chamber humidity and thermistor probe for controlling chamber humidity. 8. Peltier heating and cooling block, which maintains chamber temperature. Modified after Opell, Karinshak, and Sigler, 2011.

https://doi.org/10.1371/journal.pone.0196972.g003

relative to the glycoprotein sphere's initial diameter. We generated a stress strain curve for each species glycoprotein at each humidity using mean true stress and true strain values and from this determined Young's modulus as the slope of the curve in its linear elastic phase. Toughness was computed as the area under these stress strain curves, as the sum of a series of rectangles centered at each mean stress-strain value. The Young's modulus values of flagelliform fibers reported in the literature were measured at approximately 50% RH. We did not assess how changes in humidity affect this property. Although water is known to alter the properties of spider threads [51–53], at each of our experimental humidity a viscous thread's

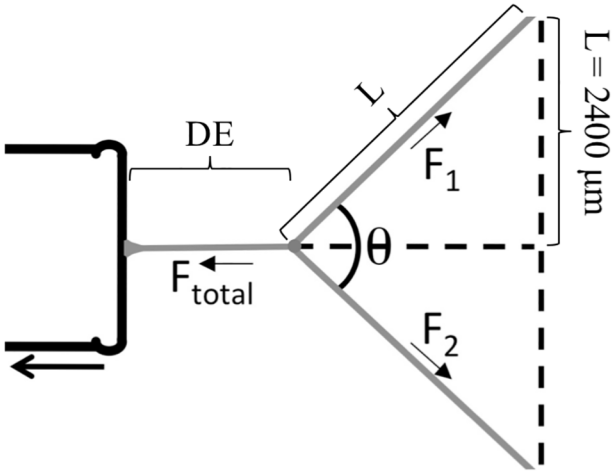

1. $L = 2400\ \mu m \div \sin(\theta/2)$
2. $AE = (L - 2400\ \mu m) \div 2400\ \mu m$
3. $F_1 = F_2 = YM \times \Sigma\, CSA_{AF} \times AE$
4. $F_{total} = 2 \times F_1 \times \sin(90° - (\theta/2))$
5. $CSA_{GF} = GV \div DE$
6. $Stress_T = F_{total} \div CSA_{GF}$
7. $Strain_T = Log_N((DE - DGC) \div DGC)$

AE = extension of axial line
YM = Young's modulus
CSA_{AF} = axial fiber cross sectional area
CSA_{GF} = glycoprotein filament cross sectional area
GV = glycoprotein volume
DGC = diameter of glycoprotein core when configured as a sphere

Each axial fiber (Sensenig et al., 2010)

	Diameter μm	Young's modulus GPa
Argiope aurantia	4.8	0.009
Neoscona crucifera	3.0	0.010
Verrucosa arenata	1.5	0.098

Fig 4. Values and formulas used to characterize glycoprotein performance and material properties.

https://doi.org/10.1371/journal.pone.0196972.g004

flagelliform fibers as well as its glycoprotein core remained coated by the thread's aqueous material.

Confirming experimental procedures

Before deriving values from stress strain curves, we assessed the efficacy of our experimental procedures and evaluated droplet extensions to ensure that they met expectations and the assumptions of our modeling. S1–S3 Tables report experimental humidities, confirming that these closely matched target humidities. Even at full droplet extension flagelliform axial fibers on each side of a droplet did not extend more than 21% of their initial in-web lengths (S4 Table), indicating that flagelliform fibers were within their linear elastic region and could reliably be used to gauge the force on an extending droplet.

In a subsequent experiment, we examined the possibility that capture threads slipped through the carbon tape matrix as force was applied to a droplet thereby, compromising our method of determining the force on an extending glycoprotein filament. We compared the responses of threads attached only by carbon tape with thread to which we then applied a small drop of Elmer's Glue™, a technique that has been shown to firmly secure threads [44, 54]. We did this at 30, 50, 70, and 90% RH for threads from the webs of six individuals of each species, measuring the axial line angle just before droplets began to extend, at 50% droplet

extension, and at full extension. We also viewed movies with iMovie™ to determine the total time that the axial lines that supported an extending droplet was under tension as gauged by an angular deflection less than 180˚. Comparisons of both the angles of axial line deflection and the durations of taut droplet extensions of the two treatments showed that only for *A*. *aurantia* threads at 90% RH was there evidence for thread slippage though tape, as denoted by a significant difference between the two treatments (S5 Table). Therefore, only *A*. *aurantia* threads at 90% RH results need be excluded from consideration.

Addressing droplet formation on extending glycoprotein filaments

When droplets of a thread span extend, their glycoprotein cores remain covered by aqueous material because their individual extensions are limited by stiffness of the thread's flagelliform fibers (Fig 2). This was also the case of during the initial extension phase of the isolated, single droplets that we studied. However, as droplet extension progressed, the aqueous layer was progresses disrupted, exposing the glycoprotein (Fig 5). This was more evident at higher humidities, where reduced glycoprotein viscosity allowed longer droplet extensions. By drawing water away from the exposed glycoprotein regions and exposing them to evaporative loss, this disruption of the glycoprotein's aqueous sheath has the potential to dry and stiffen glycoprotein. Moreover, glycoprotein is deprived of its plasticizing LMMCs [35]. Droplets appear to form on a filament to minimize the surface energy of the thinning aqueous sheath because these droplets have a lower surface to volume ratio than that of a continuous cylinder of aqueous material, a phenomenon described by Plateau-Rayleigh instability [19]. We evaluated this by computing a ratio of the circumference of what would have been a continuously aqueous layer coated glycoprotein filament divided by the cross-sectional area of the aqueous layer. We did this by dividing the volume of each component by the length of the extended droplet and positioning the glycoprotein filament in the center of the aqueous layer. As circumference is proportional to the aqueous layer's surface tension, dividing this by aqueous volume yields an index whose increase is directly related to the instability of the aqueous layer and the likelihood that droplets will from on the glycoprotein filament. Plots show that this ratio increases both as humidity increases and as the length of an extending droplet increases (Fig 6).

These observations and models indicate that the onset of droplet formation can be identified as a pronounced increase in the slope of a droplet's stress-strain curve, a prediction that was supported (Fig 7). This signature allows us to identify two phases of droplet extension and to compute separate *E* and toughness values for each phase. Phase 1 occurs early in droplet extension when glycoprotein is fully enclosed in the aqueous layer and corresponds to the normal glycoprotein performance where droplet length is constringed by the stiffness of the thread's flagelliform fibers (Fig 2). Phase 2 begins when portions of the glycoprotein filaments are exposed as droplets form. Table 1 identifies the limits of Phase 1 and Phase 2 portions of each species' stress strain curves. Toughness values were separately computed for the areas under Phase 1 and Phase 2 regions of each stress-strain curve. Only *A*. *trifasciata* exhibited reliable values for 20% RH, as *Neoscona crucifera* droplets did not extend at 20% RH and only four *V*. *arenata* droplets extended at this humidity.

Results

S6–S8 Tables summarize the three species' axial line deflections, computed forces on extended droplets, and droplet lengths from 25%—full extensions. S9 Table provides Phase 1 and Phase 2 stress, strain, Young's modulus, and toughness values for all individuals of each species at each RH. In all intra-specific and inter-specific comparisons of *E* and toughness most values were not normally distributed (Shapiro-Wilk W Tests $P \leq 0.05$). Therefore, we used Wilcoxon

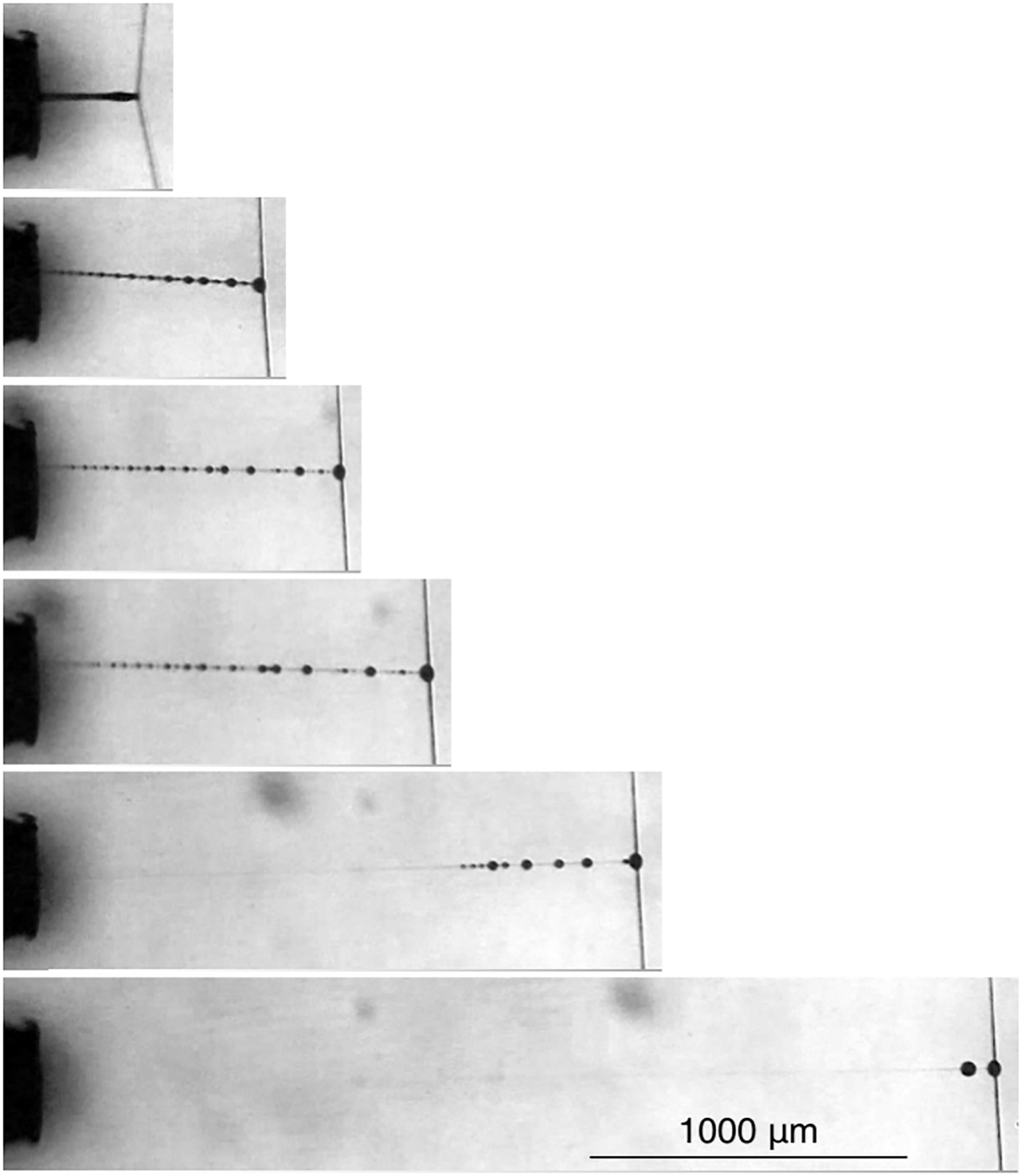

Fig 5. Progressive extension of an individual *A. aurantia* droplet, showing the formation of aqueous layer droplets on the glycoprotein filament.

https://doi.org/10.1371/journal.pone.0196972.g005

Tests to identify differences in values and, when differences were identified, Wilcoxon Each Pair Tests to rank values, considering $P \leq 0.05$ to be significant. Figs 7 and 8 compare the effect of RH on the *E* and toughness values of the three species glycoproteins. In *A. aurantia* both Phase 1 and Phase 2 *E* decreased with humidity, although this was significant only for Phase 2

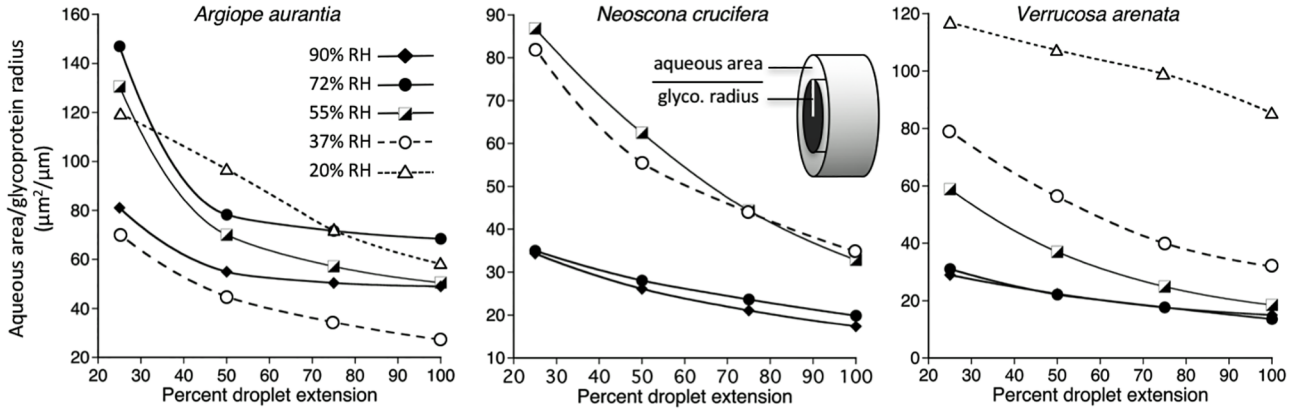

Fig 6. The effects of humidity and extension on the ratio of a glycoprotein filament's circumference to the area of its aqueous layer. As surface tension is related to circumference, an increase in this index favors the formation of aqueous droplets like those shown in Fig 5.

https://doi.org/10.1371/journal.pone.0196972.g006

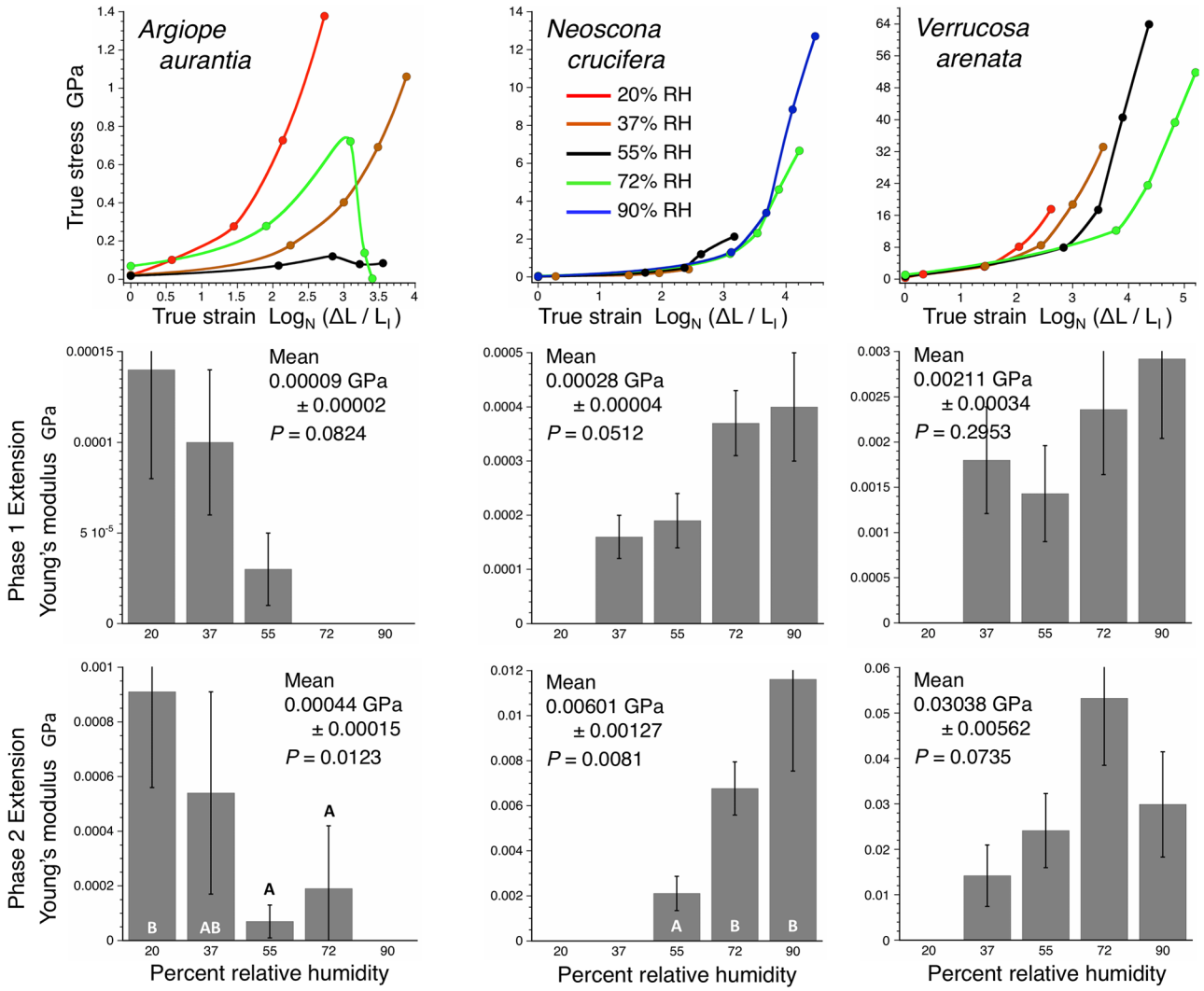

Fig 7. Stress-strain curves and Young's modulus values derived from Phase 1 and Phase 2 region of stress-strain curves. Histogram error bars are ± 1 standard error. Grand means and standard errors are given for each species' values and the *P* values of Wilcoxon Tests of the effect of RH on *E*. Letters denote the ranking of values that were significantly affected by RH, as determined by Wilcoxon Each Pairs Tests.

https://doi.org/10.1371/journal.pone.0196972.g007

Table 1. Percent droplet extension ranges used for computing Young's modulus (*E*) and percent droplet extension ranges summed to determine toughness (T) values for Phase 1 and Phase 2 of droplet extension.

	20% RH	37% RH	55% RH	72% RH	90% RH
Argiope aurantia					
E Phase 1	0–50%	0–25%	0–25%	- - -	- - -
E Phase 2	50–100%	50–100%	25–50%	25–50%	- - -
T Phase 1	25–50%	0–25%	0–25%	- - -	- - -
T Phase 2	50–100%	25–100	25–100%	0–100%	- - -
Neoscona crucifera					
E Phase 1	- - -	0–100%	0–50%	0–25%	0–25%
E Phase 2	- - -		50–100%	50–100%	50–100%
T Phase 1	- - -	0–100%	0–50%	0–25%	0–25%
T Phase 2	- - -	- - -	50–100%	25–100%	25–100
Verrucosa arenata					
E Phase 1	- - -	0–50%	0–25%	0–25%	0–25%
E Phase 2	- - -	50–100%	50–100%	50–100%	50–100%
T Phase 1	- - -	0–25%	0–25%	0–25%	0–25%
T Phase 2	- - -	25–100	25–100%	25–100%	25–100%

https://doi.org/10.1371/journal.pone.0196972.t001

values. In *N. crucifera*, both Phase 1 and Phase 2 *E* increased with humidity, although Phase 1 differences were only marginally significant. *Verrucosa arenata E* did not differ significantly, with Phase 1 values showing little change and Phase 2 values increasing to 72% RH and then decreased. In *A. aurantia*, only Phase 2 toughness differed with humidity, a result that can be

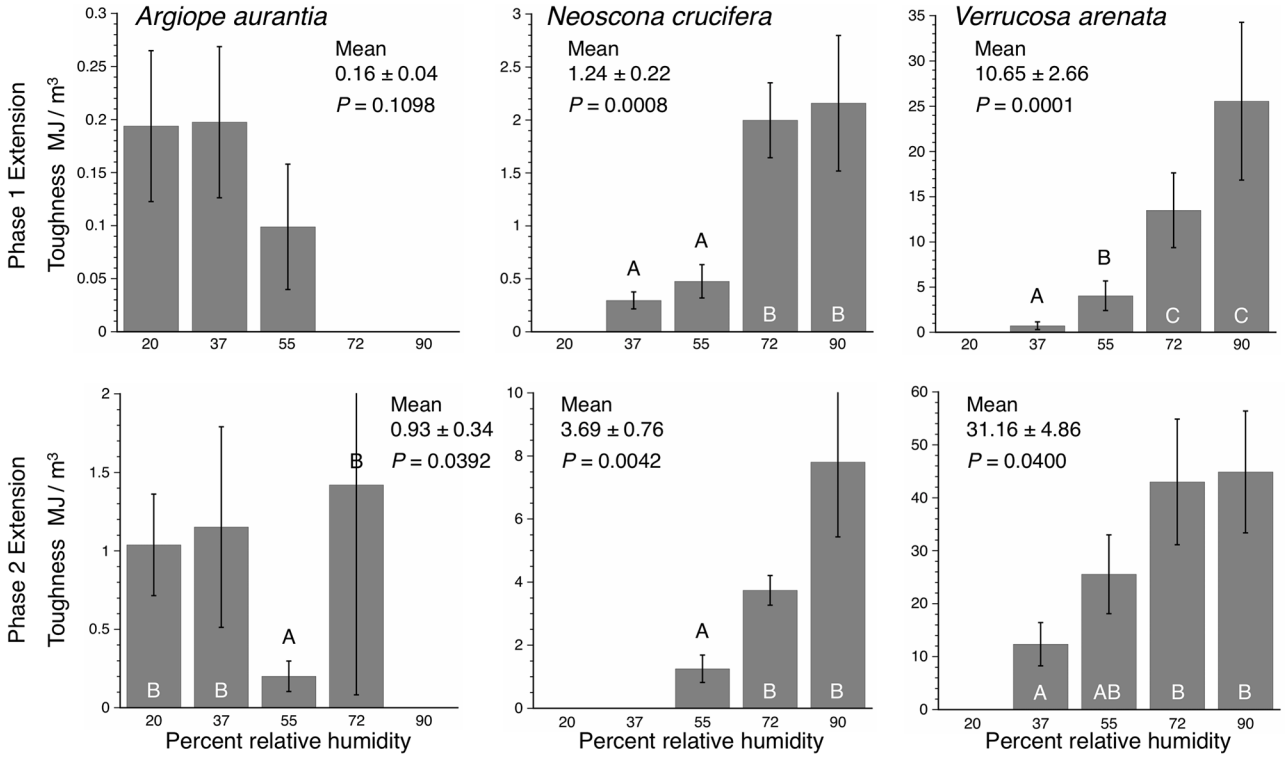

Fig 8. Toughness values derived from Phase 1 and Phase 2 region of stress-strain curves. Histogram error bars are ± 1 standard error. Grand means and standard errors are given for each species' values and the *P* values of Wilcoxon Tests of the effect of RH. Letters denote the ranking of values that were significantly affected by RH, as determined by Wilcoxon Each Pairs Tests.

https://doi.org/10.1371/journal.pone.0196972.g008

Table 2. Inter-specific comparisons of Young's modulus values.

	37% RH GPa		55% RH GPa		72% RH GPa		90% RH GPa	
	Phase 1	Phase 2	Phase 1	Phase 2	Phase 1	Phase 2	Phase 1	Phase 2
Argiope aurantia								
	A	A	A	A		A		
Neoscona crucifera								
	AB		B	B	A	B	A	
Verrucosa arenata								
	C	B	C	C	B	C	B	
Wilcoxon *P*	0.0001	0.0001	0.0001	0.0001	0.0046	0.0001	0.0015	0.8919

Letters A–C identify inter-specific ranking (low to high values) of Young's modulus as determined by Wilcoxon Each Pairs Tests.

https://doi.org/10.1371/journal.pone.0196972.t002

Table 3. Inter-specific comparisons of toughness values.

	37% RH GPa		55% RH GPa		72% RH GPa		90% RH GPa	
	Phase 1	Phase 2	Phase 1	Phase 2	Phase 1	Phase 2	Phase 1	Phase 2
Argiope aurantia								
		A	A	A		A		
Neoscona crucifera								
			B	B	A	B	A	A
Verrucosa arenata								
		B	C	C	B	C	B	B
Wilcoxon *P*	0.5794	0.0002	0.0001	0.0001	0.0147	0.0001	0.0004	0.0209

Letters A–C identify inter-specific ranking (low to high values) of Young's modulus as determined by Wilcoxon Each Pairs Tests.

https://doi.org/10.1371/journal.pone.0196972.t003

attributed to a very low 55% RH value. Both Phase 1 and Phase 2 glycoprotein toughness increased with humidity in *N*. *crucifera* and *V*. *arenata*.

For humidities at which *E* and toughness could be reliably assessed these values showed an increase from *A*. *aurantia* to *N*. *crucifera* to *V*. *arenata* (Tables 2 and 3). Phase 2 *E* and toughness values were greater that Phase 1 values and in most cases Matched Pairs Tests showed this difference to be significant ($P \leq 0.05$) (Tables 4 and 5).

Fig 9 compares the material properties of the three species' glycoproteins, flagelliform fibers, and major ampullate threads. This small number of species does now support phylogenetic comparative methods and statistical tests of relationships among these values can only be

Table 4. Intra-specific comparisons of Phase 1 and Phase 2 Young's modulus values.

	20% RH	37% RH	55% RH	72% RH	90% RH
Argiope aurantia					
	0.0251	0.2355	0.3566		
Neoscona crucifera					
			0.0103	**0.0002**	**0.0150**
Verrucosa arenata					
		0.0365	**0.0067**	**0.0020**	**0.0204**

P values of Matched Pairs Tests.

https://doi.org/10.1371/journal.pone.0196972.t004

Table 5. Intra-specific comparisons of Phase 1 and Phase 2 toughness values.

	20% RH	37% RH	55% RH	72% RH	90% RH
Argiope aurantia					
	0.0077	0.0823	0.1654		
Neoscona crucifera					
			0.0418	**0.0027**	**0.0068**
Verrucosa arenata					
		0.0117	**0.0055**	**0.0044**	**0.0247**

P values of Matched Pairs Tests.

https://doi.org/10.1371/journal.pone.0196972.t005

viewed as suggestive. The only significant correlation among the web element's *E* and toughness values was between glycoprotein and flagelliform fiber Young's modulus (r = 0.998, P = 0.0319), which lends tentative support to the coordinated evolution of the glycoprotein and axial fiber stiffness.

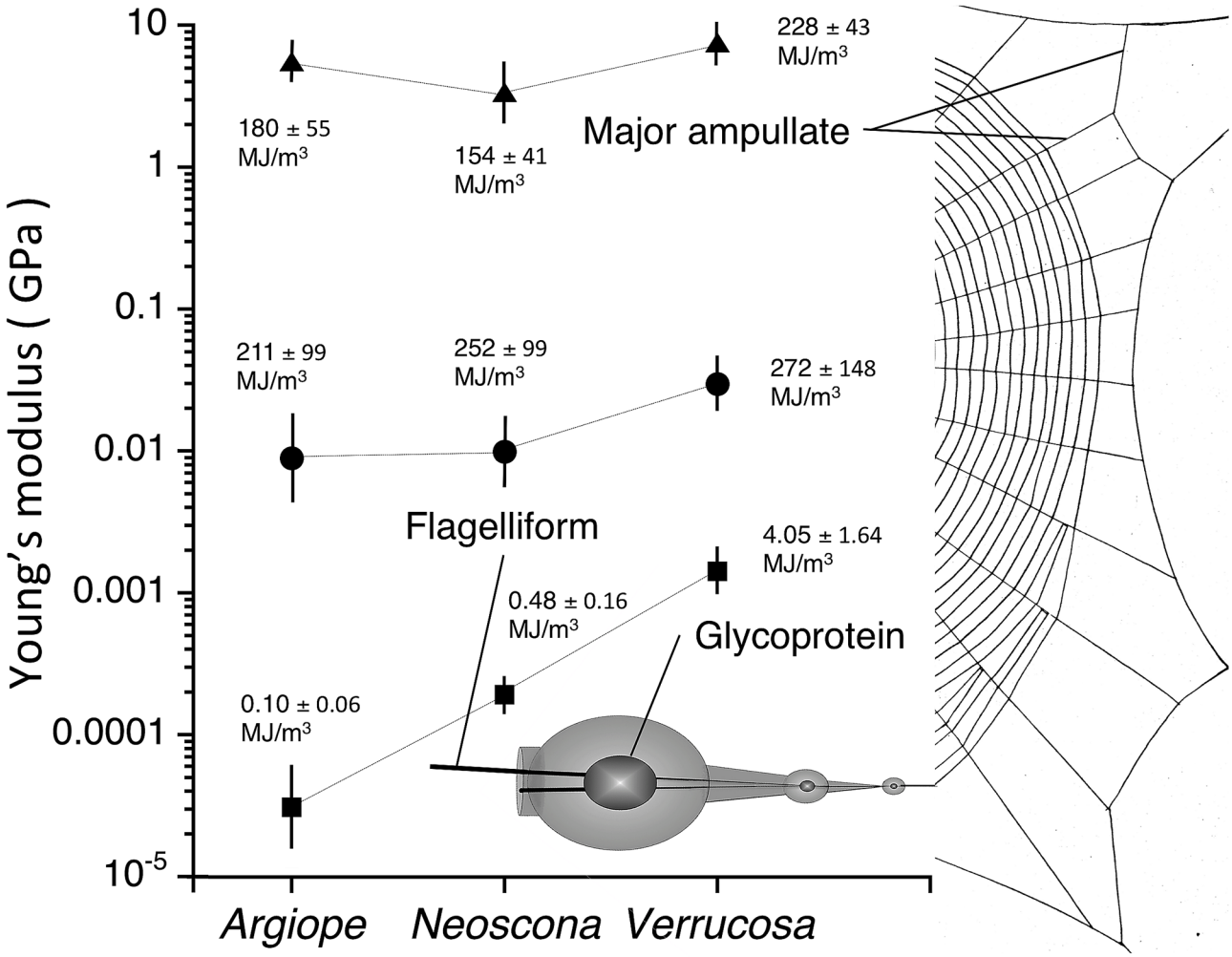

Fig 9. Comparison of 55% RH Phase 1 Young's modulus and toughness of glycoprotein from this study with flagelliform, and major ampullate fiber values measured in the range of 50% RH (Sensenig et al., 2010). Young's modulus values are plotted and described on the Y-axis. Toughness values appear beside these points. Error bars are ± 1 standard error. Lines connecting the glycoprotein, flagelliform, and major ampullate values are provided to make it easier to interpret the figure and are not regression lines.

https://doi.org/10.1371/journal.pone.0196972.g009

Discussion

As hypothesized, when compared at the same humidity, the Young's modulus of the three species' glycoproteins was less than that of their capture thread's flagelliform fibers (Fig 9). Flagelliform *E* ranged from 0.01 to 0.03 GPa [12], whereas Phase 1 glycoprotein *E* ranged from 0.00003 to 0.00140 GPa. Flagelliform values were 21, 52, and 300 times greater than Phase 1 glycoprotein values in *V*. *arenata*, *N*. *crucifer*, and *A*. *arenata*, respectively. Flagelliform fiber toughness ranged from 211–272 MJ/m^3 [12], whereas Phase 1 glycoprotein toughness ranged from 0.10–4.05 MJ/m^3. Flagelliform fiber toughness was 67, 525, and 2110 times greater than Phase 1 glycoprotein toughness in *V*. *arenata*, *N*. *crucifera*, and *A*. *arenata*, respectively. A fuller understanding of the scaling glycoprotein and flagelliform fiber *E* and its importance for the synergistic integration of capture thread components will require both a larger taxon sample and models that also incorporate data on droplet distribution, glycoprotein volume, droplet extension, and flagelliform diameter.

The apparent lack of association between *E* of major ampullate threads and the capture thread's components is not surprising, given the different roles that these web components play in prey capture. Major ampullate threads form the web's radii and function to absorb and dissipate the force when an insect strikes an orb web [13, 14]. Therefore, major ampullate threads have evolved as stiff elements. Largely freed from that task, capture threads have evolved as more compliant web elements. This allows them to conform to an insect's surface and stretch as the insect struggles to escape. The extension of both the flagelliform fibers and glycoprotein serves two purposes: it facilitates a suspension bridge mechanism that is responsible for summing the adhesive forces of multiple thread droplets [26] and it dissipates the energy of the insect's struggles [43].

When a droplet's glycoprotein is contained within its aqueous layer (Phase 1 extension), as typical during the performance of capture thread strands, *E* differs greatly among species (Fig 7), with *N*. *crucifera* E being 3.1 times that of *A*. *aurantia* and *V*. *arenata* *E* being 7.5 times that of *N*. *crucifera*. In this native state values range from 0.00003 GPa, which is similar to the *E* of fibronectin, a glycoprotein that anchors cells in the extracellular matrix [55] to 0.00292 GPa, a value similar to that of resilin in insect ligaments [56]. The ranges of Phase 1 glycoprotein *E* exhibited by *V*. *arenata* and *N*. *crucifera* were small (0.0014–0.0029 and 0.00016–0.00040 GPa, respectively), but that exhibited by *A*. *aurantia* was greater (0.00003–0.00014 GPa) (Fig 7). Although not statistically significant, these intra-specific differences suggest that glycoprotein stiffness responded to humidity.

Orb spider glycoprotein remains extensible after droplets form on the extending glycoprotein filament (Phase 2 extension). However, the glycoprotein stiffens during this phase because it was increasingly exposed to the drying effects of air. It was also deprived of LMMCs in the aqueous layer, which plasticize the glycoprotein [35]. When the aqueous layer was experimentally removed, glycoprotein adhesion at 100% RH was only half that of native droplets [35]. Moreover, Cross Polarization Magic Angle Spinning used in that study revealed that, at the molecular level, glycoprotein became more rigid and an unresponsive to changes in humidity when deprived of LMMCs. This may account for Phase 2 *E* being 4.7 times that of Phase 1 *E* in *A*. *aurantia*, 19.4 times greater in *N*. *crucifera*, and 19.2 times greater in *V*. *arenata*. Phase 2 E ranging from 0.00007 to 0.053 GPa, extending glycoprotein stiffness into the range of the proximal region of mussel threads fibers [57] and the mid-range of silicone rubber [58]. Native glycoprotein toughness ranges from 0.1 MJ/m^3 at 55% RH in *A*. *aurantia* to 26 MJ/m^3 at 90% RH in *V*. *arenata*. In these species and at these humidities Phase 2 toughness ranges from 0.2 to 45 MJ/m^3.

Conclusions

Compounds in the aqueous material that surrounds the adhesive glycoprotein cores of capture thread droplets ensures that the glycoprotein is hydrated, maintains glycoprotein integrity, and ensures glycoprotein extensibility. This extensibility combines with that of a thread's axial lines to dissipate the force of a struggling prey and sum the adhesion of multiple droplets. Our study documents the broad range of orb spider glycoprotein elastic modulus and toughness and shows that these proteins continue to exhibit desirable properties outside of their native aqueous covering. Humidity affects the material properties that a species' glycoprotein expresses, but the greatest difference is seen among species. The elastic modulus of a species' glycoprotein is much less than that of a capture thread's supporting flagelliform fibers. In our limited sample of three species, stiffer axial lines are associated with stiffer glycoproteins, suggesting that the properties of viscous capture thread components may have evolved in a synergistic fashion to optimize thread adhesion, a hypothesis that remains to be tested.

Supporting information

S1 Fig. Changes in glycoprotein volume with increasing relative humidity. When *Verrucosa arenata* volume is computed in the same manner as *Neoscona crucifera* and *Argiope aurantia* its high viscosity produces erroneous results, making it appear that volume decreases precipitously as humidity increases. When *V*. *arenata* glycoprotein volume is adjusted, these corrected values show the same trend as the other two species.
(TIF)

S2 Fig. Flattened droplet thickness, indicating a decrease in viscosity with increasing humidity. Mean ± 1 standard error. At 72% and 90% RH the standard error bars of *V*. *arenata* are hidden by its symbols.
(TIF)

S1 Table. Features of *Argiope aurantia* droplets and the humidities at which they were measured (mean ± 1 standard error). Sample size: 20% RH, 37% RH, and 55% RH = 14; 72% RH = 11; 90% = 13.
(DOCX)

S2 Table. Features of *Neoscona crucifera* droplets and the humidities at which they were measured (mean ± 1 standard error). Sample size: 37% RH = 5; 55% RH = 13; 72% RH = 12; 90% RH = 14.
(DOCX)

S3 Table. Features of *Verrucosa arenata* droplets and the humidities at which they were measured (mean ± 1 standard error). Sample size: 20% RH, = 11; 37% RH, 55% RH, 72% RH, and 90% RH = 12.
(DOCX)

S4 Table. Ranges of individual spider mean percent axial line extension at sampled droplet extension phases, with standard error of the largest value indicated.
(DOCX)

S5 Table. Comparison of axial line angles at droplet release and total loaded extension times between threads that were secured to sampler supports by carbon tape alone and those to which Elmer's® glue was subsequently added. Angles area compared at pre-extension, just prior to droplet extension, and at maximum extension. Mean ± 1 standard error,

T = *t* test for normally distributed values; W = Wilcoxon test for values that were not normally distributed.
(DOCX)

S6 Table. *Argiope aurantia* axial line deflection, computed force on extended droplet, and droplet length from 25%—Full extension. Mean ± 1 standard error.
(DOCX)

S7 Table. *Neoscona crucifera* axial line deflection, computed force on extended droplet, and droplet length from 25%—Full extension. Mean ± 1 standard error.
(DOCX)

S8 Table. *Verrucosa arenata* axial line deflection, computed force on extended droplet, and droplet length from 25%—Full extension. Mean ± 1 standard error.
(DOCX)

S9 Table. Excel® table of Phase 1 and Phase 2 stress, strain, Young's modulus, and toughness values for each test humidity.
(XLSX)

S1 Photo. An *Argiope aurantia* female attaches a capture thread to a radial line as she completes her orb web's capture spiral. In the early morning's high humidity the glue droplets of previously deposited capture threads have attracted atmospheric moisture and enlarged.
(JPG)

Acknowledgments

National Science Foundation grant IOS-1257719 supported this study.

Author Contributions

Conceptualization: Brent D. Opell, Sheree F. Andrews.

Data curation: Brent D. Opell, Mary E. Clouse, Sheree F. Andrews.

Formal analysis: Brent D. Opell, Mary E. Clouse, Sheree F. Andrews.

Funding acquisition: Brent D. Opell.

Investigation: Brent D. Opell, Mary E. Clouse, Sheree F. Andrews.

Methodology: Brent D. Opell, Mary E. Clouse, Sheree F. Andrews.

Project administration: Brent D. Opell.

Resources: Brent D. Opell.

Supervision: Brent D. Opell.

Validation: Brent D. Opell, Mary E. Clouse.

Visualization: Brent D. Opell, Mary E. Clouse.

Writing – original draft: Brent D. Opell.

Writing – review & editing: Brent D. Opell, Mary E. Clouse, Sheree F. Andrews.

References

1. Craig CL. Spider Webs and Silk: Tracing Evolution from Molecules to Genes to Phenotypes. New York: Oxford University Press; 2003. 230 p.
2. Foelix RF. The Biology of Spiders, 3rd edtion. Third ed. New York: Oxford University Press; 2011.
3. Garb JE. Spider Silk: an ancient biomaterial for 21st century research. In: Penney D, editor. Spider Research in the 21st Century. Manchester: Siri Scientific Press; 2013.
4. Garb JE, DiMauro T, Lewis RV, Hayashi CY. Expansion and intragenic homogenization of spider silk genes since the triassic: Evidence from mygalomorphae (Tarantulas and their kin) spidroins. Molecular Biology and Evolution. 2007; 24(11):2454–64. https://doi.org/10.1093/molbev/msm179 PMID: 17728281
5. World Spider Catalog. World Spider Catalog v18.5. Bern NHM, editor: http://wsc.nmbe.ch/; 2017. accessed on 09/2.2017 p.
6. Vollrath F, Selden P. The Role of Behavior in the Evolution of Spiders, Silks, and Webs. Annual Review of Ecology, Evolution, and Systematics. 2007; 38:819–46.
7. Blackledge TA, Scharff N, Coddington J, Szüts T, Wenzel J, Hayashi C, et al. Reconstructing web evolution and spider diversification in the molecular era. Proceedings of the National Academy of Science USA. 2009; 106:5229–34.
8. Dimitrov D, Benavides LR, Arnedo MA, Giribet G, Griswold CE, Scharff N, et al. Rounding up the usual suspects: a standard target-gene approach for resolving the interfamilial phylogenetic relationships of ecribellate orb-weaving spiders with a new family-rank classification (Araneae, Araneoidea). Cladistics. 2016; 33:221–50. https://doi.org/10.1111/cla.12165
9. Hormiga G, Griswold CE. Systematics, Phylogeny, and Evolution of Orb-Weaving Spiders. Annual Review of Entomology. 2014; 59:487–512. https://doi.org/10.1146/annurev-ento-011613-162046 PMID: 24160416
10. Coddington JA. Spinneret silk spigot morphology: Evidence for the monophyly of orb-weaving spiders, Cyrtophorinae (Araneidae), and the group Theridiidae plus Nesticidae. Journal of Arachnology. 1989; 17:71–96.
11. Wolff JO, Grawe I, Wirth M, Karstedt A, Gorb SN. Spider's super-glue: thread anchors are composite adhesives with synergistic hierarchical organization. Soft Matter. 2015; 11:2394–403. https://doi.org/10.1039/c4sm02130d PMID: 25672841
12. Sensenig A, Agnarsson I, Blackledge TA. Behavioral and biomaterial coevolution in spider orb webs. Journal of Evolutionary Biology. 2010; 23:1839–56. https://doi.org/10.1111/j.1420-9101.2010.02048.x PMID: 20629854
13. Sensenig A, Kelly SP, Lorentz KA, Lesher B, Blackledge TA. Mechanical performance of spider orb webs is tuned for high-speed prey. Journal of Experimental Biology. 2013; 216:3388–94. https://doi.org/10.1242/jeb.085571 PMID: 23966586
14. Sensenig A, Lorentz KA, Kelly SP, Blackledge TA. Spider orb webs rely on radial threads to absorb prey energy. Interface. 2012; 9:1880–91. https://doi.org/10.1098/rsif.2011.0851 PMID: 22431738
15. Blackledge TA, Zevenbergen JM. Mesh width influences prey retention in spider orb webs. Ethology. 2006; 112:1194–201.
16. Chacón P, Eberhard WG. Factors affecting numbers and kinds of prey caught in artificial spider webs with considerations of how orb-webs trap prey. Bulletin of the British Arachnological Society. 1980; 5:29–38.
17. Opell BD, Jain D, Dhinojwala A, Blackledge TA. Tuning orb spider glycoprotein glue performance tohabitat humidity. Journal of Experimental Biology. 2018; 221:1–12. https://doi.org/10.1242/jeb.161539 PMID: 29581217
18. Edmonds D, Vollrath F. The contribution of atmospheric water vapour to the formation and efficiency of a spider's web. Proceedings of the Royal Society of London. 1992; 248:145–8.
19. Mead-Hunter R, King AJC, Mullins BJ. Plateau Rayleigh instability simulation. Langmuir. 2012; 28:6731–5. https://doi.org/10.1021/la300622h PMID: 22512475
20. Roe R. Wetting of fine wires and fibers by a liquid film. Journal of Colloid and Interface Science. 1975; 50:70–9.
21. Dickinson GH, Vega IE, Wahl KJ, Orihuela B, Beyley V, Rodriguez EN, et al. Barnacle cement: a polymerization model based on evolutionary concepts. Journal of Experimental Biology. 2009; 212:3499–510. https://doi.org/10.1242/jeb.029884 PMID: 19837892
22. Naldrett MJ. The importance of sulphur cross-links and hydrophobic interactions in the polymerization of barnacle cement. Journal of Marine Biology Association. 1993; 73:689–702.

23. So CR, Fears KP, Leary DH, Scancella JM, Wang ZL, Liu JL, et al. Sequence basis of barnacle cement nanostructure is defined by proteins with silk homology. Scientific Reports. 2016; 6:36219. https://doi.org/10.1038/srep36219 PMID: 27824121

24. Waite JH. Mussel adhesion–essential footwork. Journal of Experimental Biology. 2017; 220:517–30. https://doi.org/10.1242/jeb.134056 PMID: 28202646

25. Opell BD, Hendricks ML. Adhesive recruitment by the viscous capture threads of araneoid orb-weaving spiders. Journal of Experimental Biology. 2007; 210:553–60. https://doi.org/10.1242/jeb.02682 PMID: 17267640

26. Opell BD, Hendricks ML. The adhesive delivery system of viscous prey capture threads spin by orb-weaving spiders. Journal of Experimental Biology. 2009; 212:3026–34. https://doi.org/10.1242/jeb.030064 PMID: 19717686

27. Townley MA, Bernstein DT, Gallangher KS, Tillinghast EK. Comparative study of orb web hydroscopicity and adhesive spiral composition in three areneid spiders. Journal of Experimental Zoology. 1991; 259:154–65.

28. Townley MA, Pu Q, Zercher CK, Neefus CD, Tillinghast EK. Small organic solutes in sticky droplets from orb webs of the spider *Zygiella atrica* (Araneae; Araneidae): β-alaninamide is a novel and abundant component. Chemistry and Biodiversity. 2012; 9:2159–74. https://doi.org/10.1002/cbdv.201200077 PMID: 23081916

29. Townley MA, Tillinghast EK. Aggregate Silk Gland Secretions of Araneoid Spiders. In: Nentwig W, editor. Spider Ecophysiology. New York: Springer-Verlag; 2013. p. 283–302.

30. Townley MA, Tillinghast EK, Neefus CD. Changes in composition of spider orb web sticky droplets with starvation and web removal, and synthesis of sticky droplet compounds. Journal of Experimental Biology. 2006; 209:1463–86. https://doi.org/10.1242/jeb.02147 PMID: 16574806

31. Opell BD, Karinshak SE, Sigler MA. Humidity affects the extensibility of an orb-weaving spider's viscous thread droplets. Journal of Experimental Biology. 2011; 214:2988–93. https://doi.org/10.1242/jeb.055996 PMID: 21832141

32. Opell BD, Karinshak SE, Sigler MA. Environmental response and adaptation of glycoprotein glue within the droplets of viscous prey capture threads from araneoid spider orb-webs. Journal of Experimental Biology. 2013; 216:3023–34. https://doi.org/10.1242/jeb.084822 PMID: 23619400

33. Sahni V, Blackledge TA, Dhinojwala A. Viscoelastic solids explain spider web stickiness. Nature Communications. 2010; 1:19 https://doi.org/10.1038/ncomms1019:1–4. PMID: 20975677

34. Sahni V, Blackledge TA, Dhinojwala A. Changes in the adhesive properties of spider aggregate glue during the evolution of cobwebs. Scientific Reports. 2011; 1:41:1–8.

35. Sahni V, Miyoshi T, Chen K, Jain D, Blamires SJ, Blackledge TA, et al. Direct solvation of glycoproteins by salts in spider silk glues enhances adhesion and helps to explain the evolution of modern spider orb webs. Biomacromolecules. 2014; 15:1225–32. https://doi.org/10.1021/bm401800y PMID: 24588057

36. Ayoub NA, Garb JE, Tinghitella RM, Collin MA, Hayashi CY. Blueprint for a high-performance biomaterial: full-length spider dragline silk genes. PLOS ONE. 2007; 2:e514. https://doi.org/10.1371/journal.pone.0000514 PMID: 17565367

37. Choresh O, Bayarmagnai B, Lewis RV. Spider web glue: two proteins expressed from opposite strands of the same DNA sequence. Biomacromolecules. 2009; 10:2852–6. https://doi.org/10.1021/bm900681w PMID: 19731928

38. Collin MA, Clarke TH, Ayoub NA, Hayashi CY. Evidence from multiple species that spider silk glue component ASG2 is a spidroin. Scientific Reports. 2016; 6:21589. https://doi.org/10.1038/srep21589 PMID: 26875681

39. Garb JE, Ayoub NA, Hayashi CY. Untangling spider silk evolution with spidroin terminal domains. BMC Evolutionary Biology. 2010; 10:243. https://doi.org/10.1186/1471-2148-10-243 PMID: 20696068

40. Gatesy J, Hayashi C, Motriuk D, Woods J, Lewis R. Extreme diversity, conservation, and convergence of spider silk fibroin sequences. Science. 2001; 291:2603–5. https://doi.org/10.1126/science.1057561 PMID: 11283372

41. Vasanthavada K, Hu X, Tuton-Blasingame T, Hsia Y, Sampath S, Pacheco R, et al. Spider glue proteins have distinct architectures compared with traditional spidroin family members. Journal of Biological Chemistry. 2012; 287:35986–99. https://doi.org/10.1074/jbc.M112.399816 PMID: 22927444

42. Peñalver E, Grimaldi DA, Delclòs X. Early cretaceous spider web with its prey. Science. 2006; 312:1761. https://doi.org/10.1126/science.1126628 PMID: 16794072

43. Piorkowski D, Blackledge TA. Punctuated evolution of viscid silk in spider orb webs supported by mechanical behavior of wet cribellate silk. The Science of Nature. 2017; 104:67. https://doi.org/10.1007/s00114-017-1489-x PMID: 28752413

44. Amarpuri G, Zhang C, Diaz C, Opell BD, Blackledge TA, Dhinojwala A. Spiders tune glue viscosity to maximize adhesion. ASC Nano. 2015; 9:11472–8.

45. Becker N, Oroudjev E, S M, Cleveland JP, Hansma PK, Hayashi CY, et al. Molecular nanosprings in spider capture-silk threads. Nature Materials 2003; 2:278–83. https://doi.org/10.1038/nmat858 PMID: 12690403

46. Stellwagen SD, Opell BD, Clouse ME. Environmental influences on the extensibility of orb-weaving spiders' adhesive, viscous droplets. Annual Meeting Proceedings of The Adhesive Society. 2015; 2015:1–3.

47. Stellwagen SD, Opell BD, Clouse ME. The impact of UVA on the glycoprotein glue of orb-weaving spider capture thread from diurnal and nocturnal species. Journal of Arachnology. 2016; 44:401–4.

48. Rasband WS. ImageJ, U. S. National Institutes of Health, Bethesda, Maryland, USA. http://imagejnihgov/ij/. 1997–2012.

49. Opell BD, Schwend HS. The effect of insect surface features on the adhesion of viscous capture threads spun by orb-weaving spiders. Journal of Experimental Biology. 2007; 210:2352–60. https://doi.org/10.1242/jeb.004952 PMID: 17575040

50. Liao C, Blamires SJ, Hendricks ML, Opell BD. A re-evaluation of the formula to estimate the volume of orb web glue droplets. Journal of Arachnology. 2015; 43:97–100.

51. Work RW. A comparative study of the supercontraction of major ampullate spider fibers of orb-weaving spiders (Araneae). Journal of Arachnology. 1981; 9:299–308.

52. Work RW. Aphysico-chemical study of the supercontraction of spider major ampullate silk fibers. Textile Research Journal. 1982; 52:349–56.

53. Agnarsson I, Dhinojwala A, Sahni V, Blackledge TA. Spider silk as a novel high performance muscle driven by humidity. Journal of Experimental Biology. 2009; 212:1990–4. https://doi.org/10.1242/jeb.028282 PMID: 19525423

54. Blackledge TA, Hayashi CY. Silken toolkits: biomechanics of silk fibers spun by the orb web spider Argiope argentata (Fabricius 1775). Journal of Experimental Biology. 2006; 209:2452–61. https://doi.org/10.1242/jeb.02275 PMID: 16788028

55. Klotzsch E, Smith ML, Kubow KE, Muntwyler S, Little WC, Beyeler F, et al. Fibronectin forms the most extensible biological fibers displaying switchable force-exposed cryptic binding sites. Proceedings of the National Academy of Science. 2009; 106:18267–72.

56. Guthold M, Liu W, Sparks E. A., Jawerth LM, Peng L, Falvo M, et al. A comparison of the mechanical and structural properties of fibrin fibers with other protein fibers. Cell Biochemistry and Biophysics. 2007; 49:165–81. https://doi.org/10.1007/s12013-007-9001-4 PMID: 17952642

57. Lucas JM, Vaccaro E, Waite JH. A molecular, morphometric and mechanical comparison of the structural elements of byssus from *Mytilus edulis* and *Mytilus galloprovincialis*. Journal of Experimental Biology. 2002; 205:1807–17. PMID: 12042339

58. Anonymous. Silicone rubber [Internet]. Manchester, UK: AZoNetwork UK Ltd.; 2001 [cited 2017 June 14]. Product description and specificaitons].